

In situ ion-microprobe determination of trace element partition coefficients for hornblende, plagioclase, orthopyroxene, and apatite in equilibrium with natural rhyolitic glass, Little Glass Mountain Rhyolite, California

JAMES G. BROPHY,^{1,*} TSUTOMU OTA,² TAK KUNIHRO,² TATSUKI TSUJIMORI,²
AND EIZO NAKAMURA²

¹Department of Geological Sciences, Indiana University, Bloomington, Indiana 47401, U.S.A.

²The Pheasant Memorial Laboratory for Geochemistry and Cosmochemistry (PML), Institute for Study of the Earth's Interior, Okayama University at Misasa, Tottori-Ken 682-0193, Japan

ABSTRACT

Partially crystalline hornblende gabbro inclusions from the Little Glass Mountain Rhyolite contain euhedral plagioclase, orthopyroxene, hornblende, and apatite crystals in contact with interstitial rhyolitic (71–76% SiO₂) glass. Textural and mineral compositional data indicate that the gabbros crystallized sufficiently slowly that surface equilibrium was closely approached at the interface between crystals and the liquid. This rare occurrence represents a natural dynamic crystallization experiment with a “run time” that is not realistically achievable in the laboratory. SIMS analysis of mineral rim-glass pairs have permitted the determination of high-quality, equilibrium trace-element partition coefficients for all four minerals. These data augment the limited partition coefficient database for minerals in high-SiO₂ rhyolitic systems. For all minerals, the D values are consistent with those anticipated from crystal-chemical considerations. These data further support a liquid SiO₂ control on the REEs (and presumably other elements) partitioning wherein D values systematically increase with increasing liquid SiO₂ content.

Keywords: Ion microprobe, rhyolite glass, trace element, partition coefficient

INTRODUCTION

Trace elements are important tools for deciphering crystallization and melting processes in igneous systems. Unfortunately, for those interested in the generation of silicic magma (i.e., > ~70% SiO₂) the volume of high-quality mineral-liquid trace element partition coefficient data (D) is significantly less than that found in mafic to intermediate systems. This is due in large part to the near ubiquitous presence of accessory mineral inclusions in mineral separates from high-SiO₂ natural lavas, thus rendering mineral-matrix based D data potentially unreliable, and to difficulties in achieving equilibrium conditions in experiments with high liquid SiO₂ contents. With the advent of in situ trace element analytical techniques [e.g., secondary ion mass spectrometry (SIMS), laser ablation inductively coupled plasma mass spectrometry (LA-ICPMS)] the analysis of coexisting phenocrysts and glassy matrix in natural high-SiO₂ lavas has eliminated the problem of accessory mineral inclusions and has led, for the first time, to reliable, high-quality distribution coefficient (D) value information in high-SiO₂ liquid systems (e.g., Sisson 1991, 1994; Ewart and Griffin 1994). However, such data are still limited in number. This study takes advantage of a natural occurrence of partially crystalline hornblende gabbros found as cognate inclusions within the Little Glass Mountain Rhyolite lava flow, Medicine Lake Volcano, California (Donnelly-Nolan et al. 1990). The gabbro inclusions contain, among other things, euhedral crystals of hornblende, orthopyroxene, plagioclase, and apatite, that are in direct contact with quenched rhyolitic glass

(~71–76% SiO₂). Previous studies (Grove and Donnelly-Nolan 1986; Brophy et al. 1996) have demonstrated that the gabbros are the result of in situ crystallization of a basaltic andesite magma, most likely in an inward-growing solidification front. Brophy et al. (1996) demonstrated that the crystallization was sufficiently slow that the constituent minerals closely approached surface equilibrium with the silicate melt throughout the crystallization process. Thus, this rare occurrence represents a natural dynamic crystallization experiment with a “run time” that is not realistically achievable in the laboratory. In this regard, these inclusions provide an ideal opportunity to acquire high-quality equilibrium D value information for hornblende, plagioclase, orthopyroxene, and apatite in high-SiO₂ liquid systems through in situ SIMS analysis of coexisting glass and minerals.

SAMPLE DESCRIPTION

The gabbro inclusions are located within the Little Glass Mountain Rhyolite, a young (~1065 yr, Donnelly-Nolan et al. 1990) calc-alkaline lava flow erupted along the southwest flanks of Medicine Lake Volcano, California. They have been the subject of multiple investigations (e.g., Mertzmann and Williams 1981; Grove and Donnelly-Nolan 1986; Brophy et al. 1996; Grove et al. 1997). The inclusions consist of an interconnected framework of plagioclase, olivine, orthopyroxene, augite, hornblende, magnetite, and ilmenite set within a matrix of vesicular, clear to dark-brown rhyolitic glass (Fig. 1). Small, euhedral apatite crystals are dispersed throughout the glass. Within a given inclusion the glass is compositionally homogeneous. From one inclusion to the next, the glass composition can

* E-mail: brophy@indiana.edu

vary from ~71 to as high as 76% SiO₂ (on an anhydrous basis). Anhedral olivine and augite are invariably mantled by euhedral orthopyroxene and hornblende, respectively. Plagioclase forms euhedral crystals, whereas ilmenite and magnetite form anhedral grains. The mineralogy and texture record a crystallization sequence wherein initial crystallization of plagioclase + olivine + augite gave way to plagioclase + orthopyroxene + hornblende + ilmenite/magnetite + apatite (Brophy et al. 1996). Two gabbro inclusions were selected for study (LGM-9 and 661M-c). Table 1 lists their whole rock major and trace element abundances.

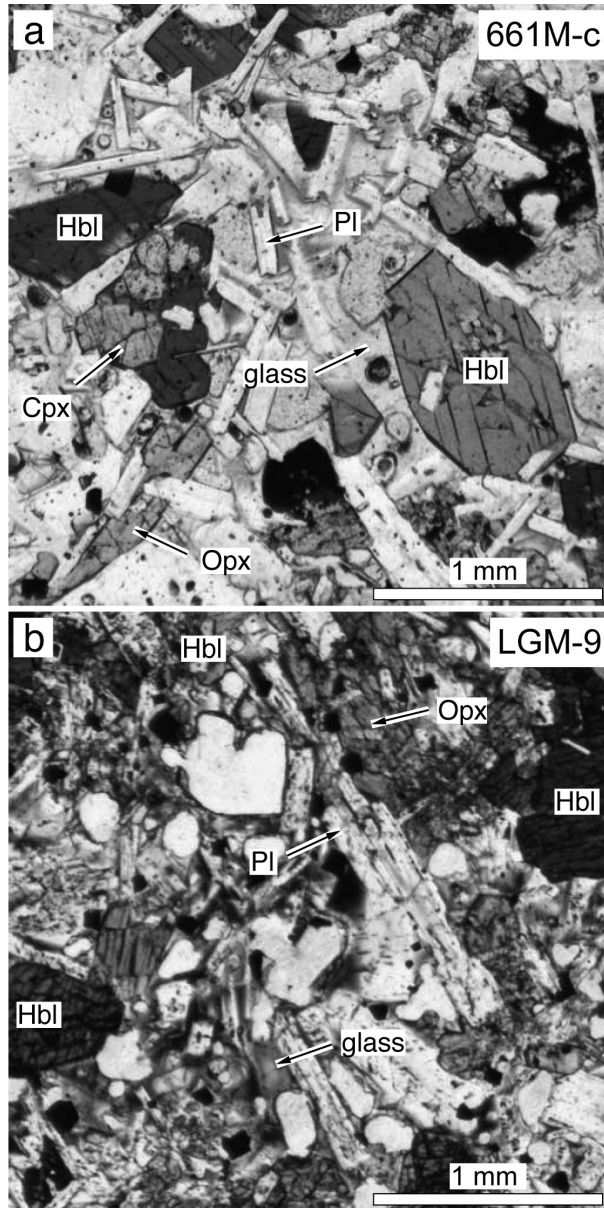


FIGURE 1. Photomicrographs of hornblende gabbro inclusions 661M-c and LGM-9. Important features to note are: (1) the interconnected framework of euhedral plagioclase and hornblende, subhedral to euhedral orthopyroxene, and anhedral Fe-oxide; (2) the euhedral hornblende overgrowth on an anhedral core of clinopyroxene; and (3) the clear, vesicular glass occupying the interstices among the crystal framework.

The two inclusions are very similar in their bulk composition. Strictly speaking, they are closer to basaltic andesite than basalt in composition with bulk SiO₂ contents approaching 54 wt%.

ANALYTICAL METHODS

Bulk rock major and trace element analyses were conducted by X-ray fluorescence spectroscopy (XRF) and LA-ICPMS at Michigan State University following the analytical procedures described in Deering et al. (2008). All glass and mineral analyses were conducted on standard 1 inch diameter circular polished thin sections. Prior to either electron microprobe analysis (EMPA) or SIMS analysis, all minerals were optically studied to identify regions that were devoid of either mineral or glass inclusions. The resultant data indicate that, at no time did the electron or ion beam pass through the mineral and into underlying glass.

Major element compositions of minerals and glass were determined by EMPA on a Cameca SX50 located at Indiana University. Operating conditions included a 15 kV acceleration voltage, 20 nA sample current and a beam diameter of 3 μm for silicate minerals, and 10 nA and 10 μm diameter beam for silicate glass. Na₂O was always analyzed first. Trace element abundances were determined by SIMS (Cameca, ims 5f) located at the Pheasant Memorial Laboratory (PML) of the Institute for Study of the Earth's Interior (ISEI), Okayama University, Misasa. Samples were sputtered with an oxygen-anion primary beam of 14–18 nA intensity resulting in a final sputtered area of 15–20 μm in diameter. Positive secondary ions were collected by ion counting using an energy offset of ~45 V from 4.5 kV acceleration. The mass calibration and estimation of elemental ion yield were carried out using in-house standards at PML. The in-house standards include andesitic (TAHITI) and basaltic (HAWAII) glass, clinopyroxene (KLB1, SAX33) and garnet (MNAG10). Trace element abundances of these standards were determined by wet chemistry with ICP-MS, following the methods described by Makishima and Nakamura (1997), Makishima et al. (1999), Yokoyama et al. (1999), and Moriguti et al. (2004). Trace elements analyzed include Li, Sr, Y, Zr, Nb, Ba, La, Ce, Pr, Nd, Sm, Eu, Gd, Dy, Er, Yb, Lu, and Hf. Among these, Li, Sr, Y, Zr, Nb, Ba, La, Ce, Pr, Nd, and Sm were analyzed by measuring the signals from one isotope, i.e., ⁷Li, ⁸⁸Sr, ⁸⁹Y, ⁹⁰Zr, ⁹³Nb, ¹³⁸Ba, ¹³⁹La, ¹⁴⁰Ce, ¹⁴¹Pr, ¹⁴⁶Nd, and ¹⁴⁹Sm. The contribution of oxide interference to the middle to heavy rare earth elements is significant. Thus, not only the ion yield of the elements of concern (X), but also the oxide-ion yield of the elements

TABLE 1. Bulk chemical compositions of the gabbroic inclusions

	LGM-9	661M-c
SiO ₂	53.93	53.64
TiO ₂	0.8	0.87
Al ₂ O ₃	17.72	17.15
FeO	6.813	7.074
MnO	0.12	0.14
MgO	5.48	5.48
CaO	8.61	8.32
Na ₂ O	3.07	3.23
K ₂ O	1.1	1.18
P ₂ O ₅	0.16	0.15
LOI	1.33	1.87
Total	99.133	99.104
Li	–	–
Sr	417	377
Y	18	21
Zr	106	117
Nb	4.45	5.81
Ba	316	295
La	10.1	9.7
Ce	22.3	22.7
Pr	2.99	3.03
Nd	12.76	13.01
Pm	–	–
Sm	2.97	3.21
Eu	1.01	1.09
Gd	3.01	3.29
Tb	0.5	0.55
Dy	2.58	3.38
Ho	0.64	0.72
Er	1.82	2.1
Yb	1.83	2.14
Lu	0.26	0.33
Hf	2.5	2.7

Notes: Major elements in wt% (cg/g). Trace elements in ppm (μg/g).

that are lighter in 16 atomic weight (Q) were estimated. Here, we assume that ion signals at mass 151, 157, 163, 167, 174, 175, and 178 are composed of $^{151}\text{Eu}^+$ and $^{135}\text{BaO}^+$, $^{151}\text{Eu}^+$ and $^{135}\text{BaO}^+$, $^{163}\text{Dy}^+$ and $^{147}\text{SmO}^+$, $^{167}\text{Er}^+$ and $^{151}\text{EuO}^+$, $^{174}\text{Yb}^+$ and $^{158}\text{GdO}^+$, $^{173}\text{Lu}^+$ and $^{159}\text{TbO}^+$, and $^{178}\text{Hf}^+$ and $^{162}\text{DyO}^+$, respectively. The abundance of Tb was estimated by interpolation of Gd and Dy in CI-chondrite normalized space. The oxide-ion yield of Q was estimated by analyzing more than two standards with different abundance ratios (Q/X). To avoid surface contamination and to obtain steady-state sputtering conditions, a target site was pre-sputtered for 120 s, and then six acquisition cycles with the following counting times per cycle: 4 s for Si; 10 s for Li, Sr, Y, and Zr; 15 s for Nb and Ba; and 20 s for La, Ce, Pr, Nd, Sm, Eu, Gd, Dy, Er, Yb, Lu, and Hf, where $^{30}\text{Si}^+$ was analyzed as internal reference. Finally trace element abundances were calculated using relative ion intensity, ion yield, oxide yield, and SiO_2 abundance that was derived from EMPA at each sputtered site. According to the repeated analysis of the standards, the overall analytical errors are $\pm 10\%$ (e.g., Nakamura and Kushiro 1998).

RESULTS

Glass and mineral major element compositions

The two gabbros selected for study contain minor olivine, augite, plagioclase, orthopyroxene, hornblende, Fe-oxides, apatite, and interstitial rhyolitic glass. LGM-9 contains magnetite, whereas 661M-c contains both magnetite and ilmenite. In both samples, anhedral olivine and augite are invariably mantled with orthopyroxene and hornblende, respectively. Average glass compositions are listed in Table 2. The glasses are typical calc-alkaline rhyolites characterized by high SiO_2 , Na_2O , and K_2O , moderate Al_2O_3 , and very low FeO, MgO, and CaO. The 661M-c glass is higher in SiO_2 than the LGM-9 glass (74.0 vs. 72.3 wt% on an anhydrous basis). Representative core and/or rim mineral compositions are listed in Tables 3 and 4. For all minerals the range of core and rim compositions are essentially the same for both samples. Olivine cores range from Fo_{66} to Fo_{72} with an average value of Fo_{68} . Augite cores show a range of $\text{Wo}_{41-43}\text{En}_{42-43}\text{Fs}_{14-16}$ with an average value of $\text{Wo}_{42}\text{En}_{43}\text{Fs}_{15}$. Orthopyroxene, which occurs either as mantles on olivine or as discrete crystals, display an average core of $\text{Wo}_3\text{En}_{67}\text{Fs}_{30}$. All crystals are normally zoned and converge toward average rim compositions of $\text{Wo}_3\text{En}_{66}\text{Fs}_{31}$. Hornblende either mantles augite or is present as discrete crystals. The average core Fe_7/Mg for both samples is 0.55. All crystals are normally zoned and converge toward an average rim Fe_7/Mg of 0.59 for both samples. Based on the classification scheme of Leake et al. (1997) the cores and rims of all hornblendes are magnesio-hornblende. Plagioclase crystals display average core compositions of around An_{72-75} . All crystals are normally zoned and converge toward

average rim compositions of An_{26} in LGM-9 and An_{24} in 661M-c. Magnetite crystals have ulvospinel contents that range from Usp_{39} to Usp_{43} . Ilmenite crystals in 661M-c have an average ilmenite content of Ilm_{89} .

Intensive parameters (P , T , f_{O_2} , XH_2O)

The recent empirical formulations of Ridolfi et al. (2010) have been used to estimate the P , T , f_{O_2} and wt% H_2O conditions just prior to eruption. Based on hornblende rim compositions, the estimated crystallization pressure was on the order of 3 kbar placing the pre-eruption magma body in the upper mid-crustal region. Estimated temperatures range from 930 to 950 °C and estimated oxygen fugacities range from $\Delta\text{NNO}+0.2-0.3$. The estimated pre-eruption H_2O content of the rhyolitic liquid is 5.5 to 5.7 wt%. Given these pre-eruption temperature and pressure estimates and the compositions of coexisting plagioclase rims and glass, the plagioclase-liquid hygrometer of Lange et al. (2009) yields a pre-eruption H_2O content of approximately 5.6 wt%, which agrees well with the estimates based on Ridolfi et al. (2010).

Glass and mineral trace element compositions

Table 5 lists the average trace element composition of glass for both samples. Also listed are average rim compositions for hornblende, orthopyroxene, plagioclase, and apatite. Multi-element and REE diagrams (Fig. 2) show that, for each sample, the glass compositions define coherent trace element patterns with minimal scatter indicating homogeneous glass compositions on the scale of a thin section. The trace element abundances of the glasses show several important features. First, relative to the bulk inclusions, the glasses display significant enrichment in Zr, Hf, and Li and marked depletion in strontium. These features are qualitatively consistent with the two-stage in situ crystallization history inferred by Brophy et al. (1996). The REE plots show that the glasses display a slight enrichment in LREEs followed by progressive depletion of the HREEs. This feature is qualitatively consistent with in situ crystallization dominated by hornblende. A striking feature of both samples is the presence of a very large positive Eu anomaly that, given the lack of any such feature in the bulk sample, must be a product of the crystallization process alone. The origin of these and other features of the glass composition are being considered elsewhere (Brophy et al. in prep).

Demonstration of surface equilibrium

On the basis of very detailed studies of trace-element zonation patterns in plagioclase crystals from similar inclusions, Brophy et al. (1996) concluded that the crystallization process was sufficiently slow that surface equilibrium was closely approached between the growing crystals and melt throughout the crystallization process. In essence, this means that crystal growth rates were slower than cation diffusion rates in the liquid, thus permitting the liquid composition at the crystal liquid interface to be the same as that of the bulk liquid at any given time. This implies that any measured trace element partition coefficients represent true equilibrium values. Because this assumption is critical to the quality of any measured partition coefficients it is important to validate it. One test of the surface equilibrium assumption is to determine the presence or absence of compo-

TABLE 2. Average glass compositions

	LGM-9*	661M-c*
SiO_2	71.92	73.54
TiO_2	0.53	0.44
Al_2O_3	14.86	14.15
FeO	1.85	1.45
MnO	0.05	0.02
MgO	0.26	0.13
CaO	0.84	0.58
Na_2O	4.39	4.34
K_2O	4.81	4.68
P_2O_5	-	-
H_2O	-	-
Total	99.51	99.33
$(\text{SiO}_2)_N$	72.27	74.04

Notes: major elements in wt% (cg/g). $(\text{SiO}_2)_N$ = anhydrous basis.

* Average of 10 random analyses.

TABLE 3. Average silicate mineral compositions

	Olivine		Augite		Orthopyroxene				Amphibole				Plagioclase			
	LGM-9 core	661M-c core	LGM-9 core	661M-c core	LGM-9 core	LGM-9 rim	661M-c core	661M-c rim	LGM-9 core	LGM-9 rim	661M-c core	661M-c rim	LGM-9 core	LGM-9 rim	661M-c core	661M-c rim
SiO ₂ *	37.58	38.11	52.24	52.39	52.06	52.50	52.15	52.28	43.66	43.92	44.56	44.22	48.85	62.22	49.31	62.34
TiO ₂	–	–	0.71	0.50	0.29	0.27	0.29	0.23	3.60	3.43	3.12	3.33	–	–	–	–
Al ₂ O ₃	–	–	2.61	1.94	1.51	1.49	1.33	1.05	11.24	11.07	10.52	10.87	33.22	23.82	32.88	24.06
Cr ₂ O ₃	–	–	0.00	0.05	0.00	0.01	0.00	0.01	–	–	–	–	–	–	–	–
FeO	28.02	27.27	9.03	9.55	19.61	20.01	18.94	20.05	13.34	13.94	13.46	13.89	0.47	0.61	0.46	0.47
MnO	0.54	0.50	0.30	0.29	0.56	0.54	0.53	0.53	0.20	0.20	0.18	0.19	–	–	–	–
MgO	33.03	34.42	14.85	14.79	24.17	23.72	24.57	23.74	13.63	13.21	13.88	13.28	–	–	–	–
CaO	0.10	0.09	20.51	20.53	1.29	1.32	1.33	1.27	11.05	11.01	10.87	10.89	15.30	5.11	14.63	4.82
Na ₂ O	–	–	0.30	0.37	0.03	0.08	0.03	0.05	2.49	2.47	2.41	2.43	2.77	7.48	3.14	7.88
K ₂ O	–	–	–	–	–	–	–	–	0.50	0.55	0.46	0.53	0.08	0.85	0.09	0.90
H ₂ O	–	–	–	–	–	–	–	–	2.07	2.06	2.07	2.06	–	–	–	–
Cl	–	–	–	–	–	–	–	–	0.02	0.02	0.02	0.03	–	–	–	–
Total	99.27	100.40	100.55	100.41	99.53	99.93	99.18	99.22	101.79	101.87	101.55	101.73	100.69	100.09	100.51	100.47
Si	1.017	1.014	1.929	1.939	1.921	1.934	1.925	1.940	6.220	6.270	6.338	6.309	2.215	2.781	2.235	2.767
Ti	0.000	0.000	0.020	0.014	0.008	0.007	0.008	0.007	0.386	0.369	0.333	0.358	0.000	0.000	0.000	0.000
^{IV} Al	0.000	0.000	0.071	0.061	0.066	0.065	0.058	0.046	1.780	1.730	1.662	1.691	1.775	1.255	1.756	1.257
^{VI} Al	0.000	0.000	0.043	0.024	0.000	0.000	0.000	0.000	0.107	0.133	0.100	0.137	0.000	0.000	0.000	0.000
Cr	0.000	0.000	0.000	0.001	0.000	0.000	0.000	0.000	–	–	–	–	–	–	–	–
Fe ³⁺	0.000	0.000	0.011	0.035	0.078	0.058	0.077	0.064	0.749	0.707	0.834	0.741	0.000	0.000	0.000	0.000
Fe ²⁺	0.634	0.607	0.267	0.261	0.527	0.558	0.507	0.558	0.840	0.957	0.767	0.916	0.018	0.023	0.018	0.017
Mn	0.012	0.011	0.009	0.009	0.018	0.017	0.017	0.017	0.024	0.024	0.022	0.023	0.000	0.000	0.000	0.000
Mg	1.333	1.365	0.817	0.816	1.330	1.303	1.352	1.314	2.894	2.811	2.943	2.825	0.000	0.000	0.000	0.000
Ca	0.003	0.003	0.811	0.814	0.051	0.052	0.053	0.051	1.687	1.684	1.656	1.665	0.743	0.245	0.710	0.229
Na	–	–	0.021	0.027	0.002	0.006	0.002	0.004	0.688	0.684	0.666	0.673	0.244	0.648	0.276	0.678
K	–	–	–	–	–	–	–	–	0.091	0.100	0.083	0.096	0.005	0.048	0.005	0.051
Cl	–	–	–	–	–	–	–	–	0.005	0.006	0.005	0.003	–	–	–	–
OH	–	–	–	–	–	–	–	–	1.995	1.994	1.995	1.997	–	–	–	–
(Fe ²⁺ +Fe ³⁺)/Mg	0.476	0.445	0.341	0.362	0.455	0.473	0.432	0.474	0.549	0.592	0.544	0.587	–	–	–	–
Fe ²⁺ /Mg	0.476	0.445	0.327	0.319	0.396	0.429	0.375	0.425	0.290	0.340	0.261	0.324	–	–	–	–
Mg/(Mg+Fe ²⁺ +Fe ³⁺)	0.678	0.692	0.753	0.758	0.716	0.700	0.727	0.702	0.775	0.746	0.793	0.755	–	–	–	–
Mg/(Mg+Fe ²⁺)	0.186	0.203	0.989	0.989	0.744	0.761	0.756	0.761	0.753	0.986	0.987	0.986	–	–	–	–
Fe ³⁺ /(Fe ²⁺ +Fe ³⁺)	0.000	0.000	0.042	0.134	0.149	0.104	0.152	0.115	0.471	0.425	0.521	0.447	–	–	–	–
Te	0.62	0.57	–	–	–	–	–	–	–	–	–	–	–	–	–	–
Fo	67.24	68.74	–	–	–	–	–	–	–	–	–	–	–	–	–	–
Fa	32.00	30.56	–	–	–	–	–	–	–	–	–	–	–	–	–	–
Ca-Ol	0.14	0.14	–	–	–	–	–	–	–	–	–	–	–	–	–	–
Wo	–	–	42.53	42.28	2.57	2.64	2.65	2.55	–	–	–	–	–	–	–	–
En	–	–	42.85	42.38	66.96	66.08	67.96	66.12	–	–	–	–	–	–	–	–
Fs	–	–	14.62	15.35	30.47	31.27	29.39	31.33	–	–	–	–	–	–	–	–
(Ca+Na) (B)	–	–	–	–	–	–	–	–	2.000	2.000	2.000	2.000	–	–	–	–
Na (B)	–	–	–	–	–	–	–	–	0.313	0.316	0.344	0.335	–	–	–	–
(Na+K) (A)	–	–	–	–	–	–	–	–	0.466	0.468	0.405	0.433	–	–	–	–
Mg/(Mg+Fe ²⁺)	–	–	–	–	–	–	–	–	0.775	0.746	0.793	0.755	–	–	–	–
Fe ³⁺ /(Fe ³⁺ + ^{VI} Al)	–	–	–	–	–	–	–	–	0.875	0.842	0.893	0.844	–	–	–	–
Ab	–	–	–	–	–	–	–	–	–	–	–	–	74.97	25.99	71.65	23.92
Or	–	–	–	–	–	–	–	–	–	–	–	–	24.56	68.86	27.83	70.76
An	–	–	–	–	–	–	–	–	–	–	–	–	0.47	5.15	0.52	5.32

sitional zonation in the quenched glasses adjacent to mineral rims, indicating equilibrium or non-equilibrium conditions, respectively. To this end, small-scale traverses were conducted across the glass-crystal interface for one crystal each of the minerals hornblende, orthopyroxene, and plagioclase in sample 661M-c. A traverse typically had 4–5 analysis points, starting in the glass ~100 µm from the crystal-liquid interface and moved toward and into the crystal with a typical spacing of ~30 µm. Figure 3 shows the data for selected compatible and incompatible, fast-diffusing and slow-diffusing trace elements from one particular hornblende traverse. Within the analytical error of each element, compositional gradients within the glass as the crystal rim is approached are absent. Given the young age of the quenched inclusions (~1065 yr) and the very slow diffusivities of ions in glass at room temperature [on the order of 10⁻²⁵–10⁻³⁰ m²/s (Watson and Baxter 2007)], the length scale over which diffusion could have eliminated existing compositional gradients is on the order of a few micrometers at best. Thus, the spatial variation

in glass composition (or lack thereof) also existed in the high-temperature liquid prior to quenching. This result is important for two reasons. First, it confirms the conclusion of Brophy et al. (1996) that crystallization was sufficiently slow such that the crystals and liquids always approached surface equilibrium conditions. Second, it permits equilibrium trace element partition coefficients to be confidently determined from SIMS analysis of adjacent mineral rims and glass.

Partition coefficients

For hornblende, plagioclase, and orthopyroxene, trace element D values were calculated for individual mineral-glass pairs by dividing the element abundance in the mineral by that in the glass. In all cases, the mineral and glass analyses were conducted immediately inboard and outboard of the mineral-glass interface, respectively. For apatite, trace-element D values were calculated by dividing the element abundance in the mineral by an average glass composition for that particular sample. The results are listed

TABLE 4. Average Fe-oxide compositions

	Magnetite		Ilmenite 661M-c
	LGM-9	661M-c	
SiO ₂ *	1.55	1.60	–
TiO ₂	13.30	14.63	46.83
Al ₂ O ₃	3.13	2.11	0.12
FeO	75.55	75.82	48.14
Cr ₂ O ₃	0.43	0.31	0.07
MnO	0.27	0.50	0.56
MgO	1.96	1.38	2.32
CaO	–	–	–
P ₂ O ₅	–	–	–
H ₂ O	–	–	–
NiO	0.04	0.03	–
Total	96.24	96.37	98.04
Si	0.057	0.059	–
Ti	0.366	0.406	0.883
Al	0.135	0.092	0.004
Fe ³⁺	1.006	0.968	0.225
Fe ²⁺	1.307	1.374	0.784
Mn	0.008	0.016	0.012
Mg	0.107	0.076	0.087
Cr	0.012	0.009	0.001
Ni	0.001	0.001	–
X _{usp} *	0.394	0.432	–
X _{lim} *	–	–	0.886

Note: Major elements in wt% (cg/g).

* From Spencer and Lindsley (1981).

in Table 6. Figures 4 and 5 show the individual D values for all minerals plotted on both multi-element and REE diagrams, respectively. Shown for comparison are other published data sets from sub-alkaline systems for which the SiO₂ content of the “liquid” (i.e., natural matrix, natural glass, or experimental glass) was reported. For these other data sets no distinction has been made among the different types of partition coefficient data (e.g., natural phenocryst-matrix, experimental, or in situ SIMS/LA-ICPMS analysis).

On the multi-element diagrams (Fig. 4) the various profiles for the two inclusions track one another perfectly. For all minerals, the D values for 661M-c (74.0% SiO₂ liquid) are slightly higher than those for LGM-9 (72.7% SiO₂). Hornblende D values show a steady increase from left to right, with most D values being greater than 1 (i.e., compatible behavior). Relative

to the overall trend, Nb and Sr display slight elevated D values, while Zr, Hf, Eu, and Li all display significantly lower values. Plagioclase D values display an essentially flat trend and, with one exception (Sr), are all incompatible. As with hornblende, Nb and Zr display a pronounced decrease, while Sr shows a very strong increase in D value. Orthopyroxene D values show a steady increase from left to right with the partitioning behavior changing from highly incompatible (e.g., Ba and Nb) to compatible (e.g., Er, Yb, Lu). Finally, apatite D values, with some notable exceptions, are all much greater than one (i.e., highly compatible behavior) and display a very slight increase from left to right. Barium, Nb, Zr, and Li display very strong decreases in D value and overall incompatible behavior. The REE diagrams (Fig. 5) emphasize many of the same features. Europium shows a significant negative anomaly in both hornblende and apatite, a moderate negative anomaly in orthopyroxene, and a moderate positive anomaly in plagioclase.

DISCUSSION

In general, our D value data compare favorably with those of previous studies, particularly with those conducted in high SiO₂ liquid systems (>70 wt%). Relative to the elements being considered, fundamental features of the various minerals would appear to be low Zr, Hf, Eu, and Li values in hornblende, low Nb and Zr and high Sr and Eu values in plagioclase, low Eu and Li values in orthopyroxene, and low Ba, Nb, Zr, Li, and Eu values in apatite. Apatite also displays a slight depletion in Sr D value. The one mineral for which our data disagree, at least in part, is orthopyroxene. Our data display a steady left to right increase in D value, changing from highly incompatible on the left to compatible on the right. This same feature is demonstrated by several of the other studies. However, there are several studies that display nearly flat, slightly incompatible or even compatible profiles. Despite these discrepancies, we are confident that our data are a true reflection of orthopyroxene partitioning behavior in, at least, high-SiO₂ liquid systems. It is worth noting that our study is one of the few to measure Li D values for hornblende and apatite. It is comforting to note that the one other study that considered the partitioning behavior of Li in hornblende also

TABLE 5. Average glass and mineral rim trace-element compositions

	LGM-9				661M-c				
	Glass	Hbl	Plag	Opx	Ap	Glass	Hbl	Plag	Opx
Li	63(1)	23.6(0.5)	9.9(0.1)	4.4(0.1)	–	46.8(0.7)	43.7(0.6)	8.9(0.5)	6.2(0.1)
Sr	31(2)	215(3)	777(9)	0.26(0.04)	693(16)	21(6)	121(1)	684(15)	0.24(0.02)
Y	24.6(0.6)	97(1)	0.29(0.02)	6.38(0.09)	697(3)	9.6(0.2)	107(1)	0.3(0.1)	15.4(0.1)
Zr	337(12)	115(1)	0.09(0.05)	3.3(0.1)	5(4)	271(7)	174(2)	0.2(3)	7.1(0.1)
Nb	12.4(0.7)	12.3(0.6)	0.02(0.02)	0.04(0.02)	0.2(0.3)	6.7(0.3)	14.6(0.6)	0.02(0.09)	0.02(0.02)
Ba	826(17)*	214(7)	101(3)	–	8(7)	765(7)	110(2)	125(6)	–
La	19.5(0.8)	8.9(0.1)	1.46(0.06)	0.04(0.02)	527(7)	12.8(0.2)	12.8(0.2)	1.9(0.1)	0.1(0.1)
Ce	42(1)	35.0(0.5)	2.4(0.1)	0.09(0.03)	1750(17)	22.8(0.4)	47.4(0.9)	3.0(0.2)	0.21(0.06)
Pr	4.7(0.1)	6.8(0.1)	0.25(0.02)	0.04(0.02)	190(3)	2.25(0.06)	8.7(0.2)	0.27(0.04)	0.039(0.004)
Nd	19.1(0.7)	41.4(0.8)	0.97(0.09)	0.26(0.09)	834(13)	8.2(0.3)	46.6(0.9)	1.1(0.2)	0.4(0.3)
Sm	3.7(0.2)	13.6(0.4)	0.2(0.1)	0.2(0.1)	191(4)	1.4(0.1)	13.1(0.4)	0.14(0.06)	0.29(0.04)
Eu	4.1(0.3)	2.9(0.1)	0.39(0.05)	0.06(0.03)	44(1)	3.5(0.3)	3.4(0.1)	0.5(0.1)	0.10(0.03)
Gd	2.5(0.6)	16.4(0.8)	0.08(0.2)	0.3(0.1)	137(12)	1.1(0.3)	13.6(0.7)	0.09(0.3)	0.6(0.1)
Dy	2.0(0.3)	16.2(0.5)	0.06(0.09)	0.78(0.07)	115(3)	0.7(0.1)	18.5(0.5)	0.04(0.05)	1.8(0.3)
Er	0.5(0.1)	8.7(0.4)	0.02(0.1)	0.9(0.1)	58(3)	0.3(0.1)	10.5(0.5)	0.02(0.03)	1.9(0.1)
Yb	0.4(0.2)	7.2(0.3)	0.013(0.06)	1.3(0.1)	43(1)	0.2(0.1)	10.9(0.4)	0.004(0.05)	3.7(0.4)
Lu	0.05(0.05)	0.91(0.08)	0.002(0.01)	0.27(0.03)	5.6(0.2)	0.02(0.07)	1.4(0.2)	0.002(0.13)	0.9(0.1)
Hf	8.3(0.6)	5.6(0.6)	0.2(0.2)	0.4(0.2)	–	4.9(0.7)	6.7(0.6)	0.6(0.4)	0.6(0.8)

Notes: Trace elements in ppm (μg/g). Numbers in parentheses indicate the 1σ error in ppm where 826(17) = 826 ± 17 ppm.

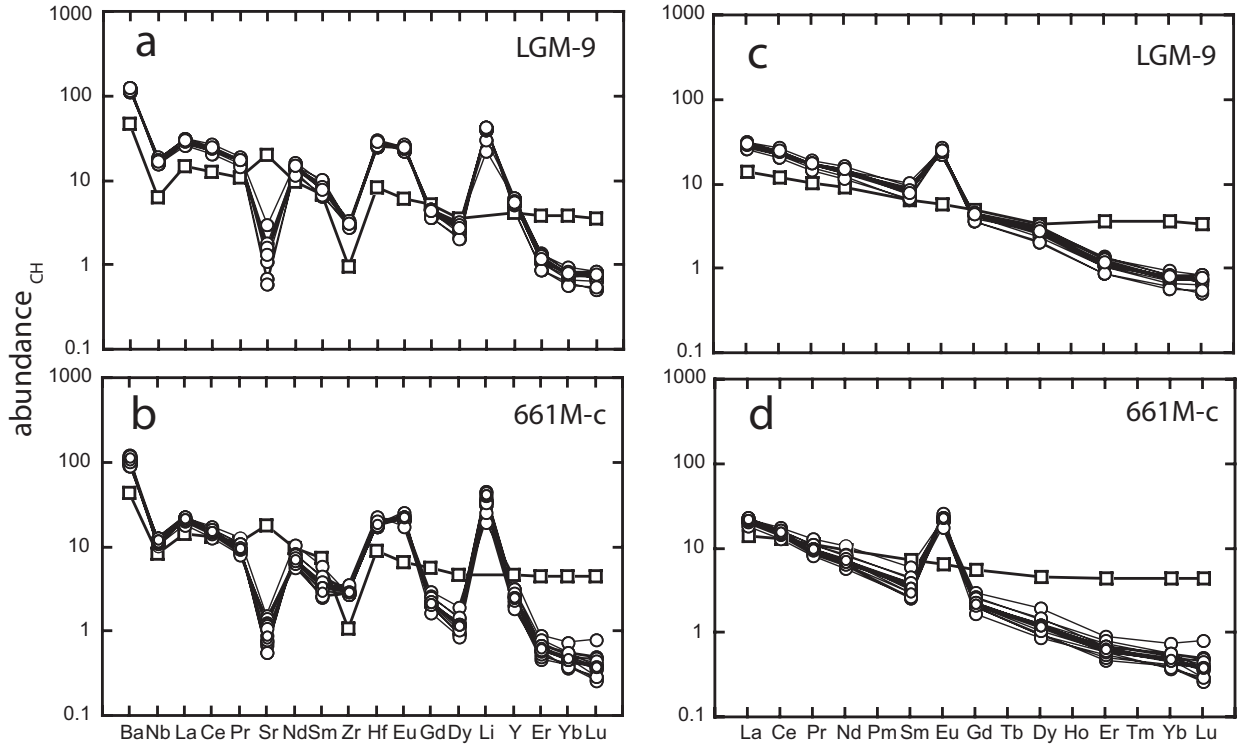


FIGURE 2. Chondrite normalized multi-element (a and b) and REE (c and d) plots for the bulk samples (open squares) and intersitial rhyolitic glass (open circles) in both inclusions.

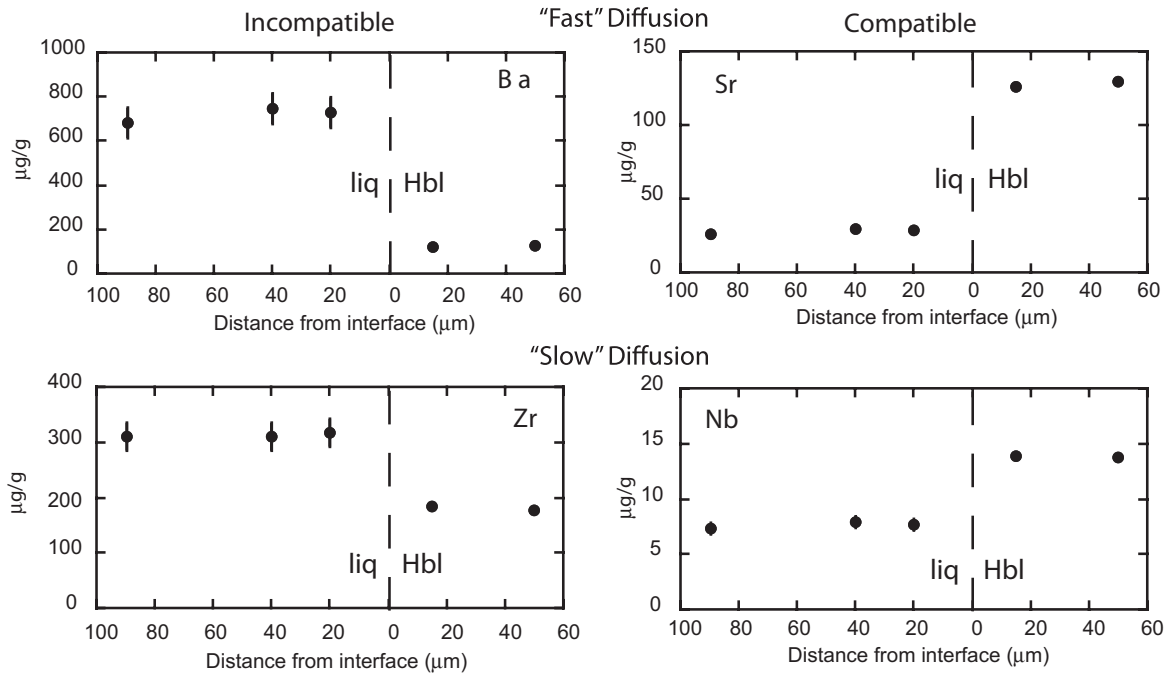


FIGURE 3. Trace element composition traverses across the mineral-glass interface for a single hornblende crystal from inclusion 661M-c. Data are shown for both incompatible and compatible and fast- and slow-diffusing elements. The error bars indicate a $\pm 10\%$ error.

TABLE 6. Calculated D values

	LGM-9 Hbl A			LGM-9 Hbl B			LGM-9 Hbl C		
	Glass	Hbl	D	Glass	Hbl	D	Glass	Hbl	D
Li	68(1)	41.3(0.9)	0.6 (0.1)	67.3(0.4)	42.2(1.0)	0.6(0.1)	68.4(0.7)	38.2(0.5)	0.56(0.06)
Sr	28.5(0.7)	179(2)	6.3(1.2)	28.9(0.5)	199.0(0.7)	6.8(0.7)	33.2(0.6)	212(3)	6.39(1.33)
Y	24.0(0.6)	111(1)	4.6(0.7)	20.2(0.3)	93.0(0.4)	4.6(0.3)	19(0.3)	94(1)	4.94(0.74)
Zr	333(17)	131(1)	0.4(0.4)	336(11)	109.0(0.4)	0.3(0.2)	309(10)	111(1)	0.36(0.21)
Nb	12.8(0.9)	15.2(0.8)	1.2(0.4)	11(0.6)	11.4(0.1)	1.0(0.2)	11.1(0.6)	12.4(0.5)	1.12(0.27)
Ba	861(7)	252(9)	0.3(0.2)	859(11)	179.0(0.6)	0.21(0.08)	834(14)	196(6)	0.24(0.15)
La	21.4(0.8)	11.1(0.1)	0.52(0.09)	19(0.5)	8.6(0.3)	0.45(0.07)	17.8(0.5)	8.6(0.2)	0.48(0.06)
Ce	44(1.8)	43.1(0.6)	1.0(0.3)	39(1)	33.3(0.9)	0.8(0.1)	36.6(0.9)	33.3(0.4)	0.91(0.15)
Pr	4.9(0.2)	8.3(0.2)	1.7(0.2)	4.3(0.1)	6.3(2.0)	1.4(0.9)	4.0(0.1)	6.5(0.1)	1.63(0.11)
Nd	19.6(0.6)	48.3(0.9)	2.5(0.5)	17.0(0.3)	37.9(0.4)	2.2(0.2)	15.5(0.4)	39.7(0.7)	2.56(0.38)
Sm	3.9(0.1)	15.6(0.5)	4.0(0.5)	2.8(0.1)	12.6(1.0)	4.5(1.1)	2.9(0.1)	13(0.3)	4.48(0.54)
Eu	4.2(0.3)	3.3(0.3)	0.8(0.2)	4.0(0.3)	2.7(0.5)	0.7(0.2)	4.1(0.3)	2.8(0.1)	0.68(0.09)
Gd	2.7(0.6)	18.5(0.9)	6.8(2.8)	2.2(0.5)	15.0(0.4)	6.8(2.4)	2.2(0.4)	18.9(0.4)	8.59(2.22)
Dy	2.1(0.2)	18.8(0.4)	8.9(1.4)	1.6(0.2)	15.2(1.0)	9.5(3.0)	1.5(0.1)	15.5(0.2)	10.33(1.30)
Er	0.53(0.2)	9.4(0.4)	17.7(5.4)	0.42(0.2)	8.3(0.3)	20(6)	0.42(0.20)	8.3(0.7)	19.76(7.89)
Yb	0.39(0.19)	8.7(0.3)	22.3(7.5)	0.3(0.1)	6.9(0.1)	23(4)	0.28(0.16)	6.7(0.3)	23.93(7.58)
Lu	0.06(0.05)	1.2(0.1)	20.0(4.5)	0.04(0.02)	0.74(0.12)	18(2)	0.04(0.02)	0.79(0.04)	19.75(2.24)
Hf	9.1(1.0)	6.4(0.5)	0.7(0.3)	7.7(0.6)	4.7(0.1)	0.6(0.1)	7.9(0.8)	5.6(1.1)	0.71(0.38)
	LGM-9 Opx A			LGM-9 Opx B			LGM-9 Opx C		
	Glass	Opx	D	Glass	Opx	D	Glass	Opx	D
Li	64.5(1.3)	4.8(0.4)	0.07(0.02)	66.3(0.5)	4.2(0.1)	0.063(0.005)	66.0(4.5)	4.50(0.09)	0.068(0.005)
Sr	30.8(2.7)	0.25(0.03)	0.008(0.004)	31(1)	0.24(0.03)	0.007(0.002)	33.8(0.7)	0.25(0.02)	0.007(0.001)
Y	23.7(0.3)	5.43(0.05)	0.23(0.02)	23.8(0.8)	5.04 (0.06)	0.21(0.003)	25.8(0.5)	5.50(0.06)	0.21(0.02)
Zr	319(8)	2.8(0.1)	0.009(0.004)	318(9)	2.80(0.07)	0.009(0.004)	343(12)	2.40(0.04)	0.007(0.004)
Nb	11.7(0.6)	0.030(0.005)	0.0025(0.0004)	12.0(0.5)	0.02(0.01)	0.0017(0.0003)	12.7(0.8)	0.09(0.02)	0.007(0.001)
Ba	874(20)	0.20(0.08)	0.0002(0.0002)	889(9)	–	–	804(14)	–	–
La	19.8(0.7)	0.020(0.003)	0.0010(0.0002)	18.4(0.4)	–	–	19.9(0.6)	0.01(0.03)	0.0005(0.0002)
Ce	42.5(1.5)	0.13(0.05)	0.0030(0.0008)	39.4(0.9)	0.050(0.004)	0.0013(0.0002)	42.0(1.3)	0.06(0.02)	0.0014(0.0003)
Pr	4.7(0.1)	0.030(0.005)	0.0064(0.0005)	4.6(0.1)	0.010(0.007)	0.0013(0.0002)	4.9(0.2)	0.06(0.02)	0.012(0.001)
Nd	19.5(0.6)	0.25(0.05)	0.013(0.002)	18.5(0.3)	0.02(0.05)	0.0011(0.0004)	20.3(0.6)	0.20(0.05)	0.009(0.001)
Sm	3.4(0.2)	0.16(0.26)	0.05(0.03)	3.7(0.2)	0.05(0.06)	0.013(0.004)	3.7(0.2)	0.14(0.09)	0.04(0.01)
Eu	4.4(0.2)	0.050(0.005)	0.011(0.001)	4.5(0.2)	0.08(0.08)	0.0178(0.005)	4.0(0.2)	–	–
Gd	2.5(0.6)	0.30(0.04)	0.12(0.05)	2.4(0.4)	0.03(0.03)	0.013(0.003)	2.6(0.7)	0.17(0.11)	0.06(0.03)
Dy	1.7(0.3)	0.66(0.04)	0.39(0.08)	2.0(0.2)	0.55(0.07)	0.28(0.05)	2.2(0.3)	0.64(0.04)	0.29(0.06)
Er	0.5(0.2)	0.85(0.06)	1.7(0.5)	0.5(0.2)	0.50(0.10)	1.0(0.3)	0.62(0.2)	–	–
Yb	0.33(0.06)	1.13(0.04)	3.3(0.4)	0.3(0.2)	1.1(0.2)	3(1)	0.4(0.3)	1.1(0.1)	2.9(1.1)
Lu	0.05(0.10)	0.23(0.02)	4.6(2.0)	0.05(0.02)	0.20(0.04)	4.0(0.6)	0.06(0.03)	0.20(0.02)	3.3(0.4)
Hf	8.0(0.5)	0.37(0.08)	0.05(0.01)	7.7(0.4)	0.2(0.1)	0.03(0.01)	9.0(0.6)	0.73(0.03)	0.08(0.02)
	LGM-9 Pl A			LGM-9 Pl B			661M-c Pl A		
	Glass	Pl	D	Glass	Pl	D	Glass	Pl	D
Li	64.70(0.08)	9.85(0.07)	0.152(0.004)	64.8(0.5)	10.50(0.08)	0.15(0.01)	53.8(0.4)	8.5(0.1)	0.16(0.01)
Sr	12(8)	836(9)	67(169)	30.7(0.2)	837(7)	27(6)	23.4(0.3)	737(8)	31(9)
Y	23.35(0.04)	0.36(0.1)	0.0155(0.0004)	25.6(0.3)	0.30(0.02)	0.012(0.001)	13.25(0.08)	0.32(0.03)	0.024(0.001)
Zr	352(1)	0.06(0.02)	0.00017(0.00001)	337(13)	0.065(0.005)	0.0002(0.0001)	400(9)	0.55(0.03)	0.0012(0.0005)
Nb	12.10(0.04)	0.035(0.007)	0.0025(0.0001)	12.6(0.7)	0.02(0.01)	0.0016(0.0003)	9.4(0.4)	0.05(0.01)	0.0053(0.0006)
Ba	782(2)	145(5)	0.19(0.07)	824(9)	205(5)	0.2(0.1)	632(3)	197(2)	0.31(0.06)
La	19.60(0.04)	2.9(0.1)	0.148(0.009)	19.5(0.5)	3.40(0.09)	0.17(0.02)	15.6(0.2)	3.3(0.2)	0.21(0.02)
Ce	42.0(0.1)	4.6(0.2)	0.110(0.009)	41(1)	5.3(0.1)	0.13(0.02)	29.3(0.7)	4.8(0.1)	0.16(0.02)
Pr	4.70(0.06)	0.45(0.06)	0.096(0.008)	4.7(0.2)	0.52(0.02)	0.110(0.008)	2.85(0.08)	0.40(0.08)	0.14(0.02)
Nd	19.2(0.1)	1.8(0.1)	0.094(0.008)	19.2(0.6)	1.80(0.09)	0.09(0.01)	9.7(0.2)	1.60(0.04)	0.16(0.01)
Sm	3.6(0.2)	0.36(0.09)	0.10(0.02)	3.8(0.1)	0.35(0.02)	0.079(0.005)	1.5(0.3)	0.2(0.2)	0.12(0.05)
Eu	4.0(0.02)	0.62(0.04)	0.155(0.008)	4.1(0.2)	0.83(0.07)	0.20(0.2)	3.0(0.2)	0.80(0.07)	0.27(0.03)
Gd	2.6(0.6)	0.17(0.2)	0.06(0.04)	2.6(0.5)	0.1(0.1)	0.05(0.02)	1.2(0.2)	0.2(0.3)	0.1(0.1)
Dy	1.9(0.2)	0.12(0.06)	0.06(0.01)	2.2(0.2)	0.10(0.01)	0.045(0.006)	0.8(0.3)	0.03(0.01)	0.04(0.01)
Er	0.53(0.08)	0.03(0.02)	0.06(0.07)	0.5(0.2)	0.03(0.01)	0.05(0.03)	0.3(0.1)	0.03(0.01)	0.1(0.1)
Yb	0.39(0.2)	0.01(0.04)	0.03(0.01)	0.4(0.2)	0.01(0.03)	0.025(0.009)	0.2(0.3)	0.005(0.01)	0.02(0.03)
Lu	0.05(0.03)	0.002(0.02)	0.04(0.02)	0.05(0.03)	0.003(0.007)	0.06(0.01)	0.02(0.05)	0.003(0.03)	0.15(0.09)
Hf	7.9(0.1)	0.3(0.2)	0.04(0.01)	8.1(0.6)	0.4(0.2)	0.05(0.02)	7.1(0.9)	1.6(1.6)	0.2(0.3)

reported a small Li D value.

An important question is whether or not our reported D values are consistent with those predicted by crystal-chemical considerations. In D vs. ionic radius plots [i.e., the PC-IR or “Onuma Diagram” of Onuma et al. (1968)] major and trace element cations with the same charge should describe smooth “bell-shaped” curves centered on the optimum size of the cation site in which the elements reside. Such diagrams are useful to determine any erratic partitioning behavior as well the particular cation site in which a given trace element resides. Figure 6 shows

D vs. ionic radius diagrams for individual crystals of hornblende, orthopyroxene, plagioclase, and apatite from inclusion LGM-9. If, for a given cation site, D values are available for two or more elements with the same charge, a qualitative bell-shaped curve was fit to the data. Overall the results in Figure 6 indicate that our measured partition coefficient values for all minerals are consistent with those expected from crystal-chemical considerations. In hornblende, the high field strength elements (HFSE) such as Hf, Zr, Nb, and Ti clearly reside in the similar sized M1, M2, and M3 sites, whereas the REEs (and Y) reside in the

TABLE 6.—EXTENDED

661M-c Hbl A			661M-c Hbl B			661M-c Hbl C		
Glass	Hbl	D	Glass	Hbl	D	Glass	Hbl	D
56.6(0.7)	55.8(0.7)	0.9(0.1)	40.9(0.2)	34.7(0.9)	0.8(0.1)	66.3(0.7)	57.6(0.8)	0.9(0.1)
16.6(0.4)	119(1)	7.2(0.8)	26.8(0.3)	130(1)	4.8(0.5)	17.9(0.4)	131(1)	7(1)
12.2(0.1)	78.8(0.6)	6.4(0.4)	8.5(0.1)	78.2(0.7)	9.2(0.8)	11.4(0.1)	83.7(0.7)	7.3(0.6)
335(4)	183(3)	0.5(0.2)	311(3)	178.0(0.8)	0.57(0.09)	325(4)	177(2)	0.5(0.1)
8.4(0.3)	13.8(0.5)	1.6(0.3)	7.4(0.2)	13.8(0.4)	1.9(0.2)	8.3(0.2)	13.4(0.5)	1.6(0.2)
715(6)	100(2)	0.14(0.05)	685(2)	128(1)	0.19(0.02)	756(5)	130(2)	0.17(0.04)
14.4(0.1)	13.1(0.2)	0.91(0.05)	12.6(0.1)	12.7(0.8)	1.0(0.2)	14.5(0.1)	13.1(0.2)	0.90(0.06)
26.4(0.2)	45.9(0.9)	1.7(0.3)	22.9(0.2)	44.2(0.1)	1.93(0.09)	26.6(0.3)	46(1)	1.7(0.2)
2.7(0.03)	7.9(0.2)	2.9(0.2)	2.25(0.06)	7.6(0.8)	3(1)	2.65(0.06)	8.0(0.1)	3.1(0.2)
9.8(0.2)	39(1)	4.0(0.9)	7.8(0.2)	38.1(0.7)	4.8(0.7)	9.1(0.2)	40(1)	4.4(0.8)
1.8(0.2)	9.7(0.3)	5.4(0.9)	1.20(0.03)	10(3)	8(8)	1.65(0.07)	10.8(0.2)	6.8(0.5)
3.6(0.4)	3.25(0.08)	0.9(0.2)	3.4(0.1)	3.0(0.5)	0.9(0.2)	4.1(0.3)	3.1(0.1)	0.7(0.1)
1.3(0.3)	8.6(0.5)	6(2)	1.0(0.3)	9.3(0.3)	9(3)	1.3(0.1)	11.1(0.5)	8(2)
0.96(0.09)	13.6(0.6)	14(3)	0.64(0.09)	12.9(0.9)	20(6)	0.89(0.09)	13.9(0.4)	16(2)
0.36(0.2)	7.1(0.4)	20(7)	0.2(0.2)	7.9(0.2)	30(8)	0.3(0.1)	8.1(0.3)	26(5)
0.26(0.14)	9.1(0.4)	35(11)	0.19(0.07)	8.9(0.1)	47(7)	0.23(0.07)	9.0(0.4)	39(7)
0.03(0.03)	1.3(0.1)	43(9)	0.02(0.03)	1.1(0.2)	55(11)	0.03(0.2)	1.2(0.2)	40(53)
6.3(0.5)	7.6(1.4)	1.2(0.7)	6.5(1.0)	6.4(0.1)	1.0(0.5)	5.8(0.2)	6.1(0.6)	1.1(0.3)
LGM-9 Opx D			LGM-9 Opx E			661M-c Opx A		
Glass	Opx	D	Glass	Opx	D	Glass	Opx	D
68.2(0.4)	6.32(0.09)	0.092(0.006)	48.6(5.6)	4.40(0.08)	0.09(0.07)	71.7(0.7)	5.8(0.07)	0.081(0.007)
28.5(0.4)	0.25(0.02)	0.0088(0.0008)	39(21)	0.26(0.02)	0.01(0.02)	12.0(0.3)	0.23(0.01)	0.019(0.002)
25.3(0.7)	5.56(0.06)	0.22(0.03)	28.1(2.6)	5.60(0.05)	0.20(0.09)	14.5(0.1)	14.0(0.1)	0.96(0.05)
341(14)	3.02(0.04)	0.009(0.006)	380(2)	3.45(0.04)	0.009(0.009)	345(5)	6.7(0.1)	0.019(0.005)
12.1(0.7)	0.06(0.02)	0.005(0.001)	13.8(1.3)	0.025(0.004)	0.0014(0.0005)	9.1(3)	0.010(0.004)	0.0011(0.0001)
879(24)	0.61(0.19)	0.0007(0.0006)	797(65)	0.5(0.4)	0.0007(0.0009)	687(5)	—	—
20.3(0.8)	0.09(0.03)	0.0044(0.0009)	18.5(1.8)	0.010(0.001)	0.0005(0.0002)	15.30(0.05)	0.09(0.09)	0.006(0.002)
43.0(1.9)	0.12(0.02)	0.0028(0.0008)	42(4)	0.09(0.01)	0.002(0.001)	29.0(0.2)	0.19(0.08)	0.006(0.001)
4.9(0.2)	0.04(0.02)	0.008(0.001)	4.7(0.5)	0.07(0.04)	0.015(0.004)	3.10(0.05)	0.040(0.004)	0.0129(0.0005)
20.6(0.8)	0.36(0.05)	0.018(0.003)	19(2)	0.23(0.03)	0.012(0.001)	11.1(0.2)	0.36(0.02)	0.032(0.002)
3.5(0.1)	0.22(0.09)	0.06(0.01)	3.8(0.4)	0.14(0.03)	0.037(0.008)	2.0(0.1)	0.27(0.04)	0.13(0.01)
4.1(0.3)	0.08(0.03)	0.019(0.003)	3.7(0.4)	0.034(0.002)	0.008(0.001)	3.6(0.3)	0.11(0.04)	0.031(0.006)
2.5(0.6)	0.51(0.1)	0.20(0.08)	2.7(2.0)	0.34(0.24)	0.1(0.1)	1.5(0.5)	0.52(0.06)	0.3(0.1)
2.0(0.3)	0.79(0.03)	0.395(0.08)	2.2(0.5)	0.64(0.04)	0.3(0.1)	1.10(0.06)	1.8(0.1)	1.6(0.2)
0.6(0.2)	1.1(0.2)	1.9(0.7)	0.6(0.2)	0.8(0.10)	1.3(0.3)	0.3(0.2)	1.9(0.1)	6(2)
0.4(0.2)	1.3(0.1)	3.3(1.0)	0.5(0.4)	1.1(0.03)	2.4(1.6)	0.27(0.11)	3.7(0.5)	14(4)
0.06(0.05)	0.31(0.03)	5.2(1.1)	0.06(0.1)	0.25(0.01)	4.2(2.0)	0.04(0.08)	0.54(0.06)	13(5)
9.1(0.5)	0.52(0.03)	0.057(0.009)	8.7(0.8)	0.19(0.08)	0.022(0.007)	6.1(0.7)	0.5(0.1)	0.08(0.03)
LGM-9 Apatite-1			LGM-9 Apatite-2			LGM-9 Apatite-3		
Glass	Ap	D	Glass	Ap	D	Glass	Ap	D
66(2)	0.4(1.5)	0.005(0.01)	66(2)	0.67(0.03)	0.0102(0.0003)	66(2)	0.06(0.01)	0.0009(0.0001)
28(3)	687(3)	24(14)	28(3)	707(21)	25(118)	28(3)	685(24)	24(26)
23.2(0.7)	1027(1)	44(7)	23.2(0.7)	550(3)	24(17)	23.2(0.7)	516(4)	22(5)
330(13)	7(13)	0.02(0.1)	330(13)	4.1(0.2)	0.012(0.001)	330(13)	4.6(0.1)	0.01(0.01)
12.0(0.8)	0.1(0.08)	0.009(0.02)	12.0(0.8)	0.44(0.09)	0.037(0.006)	12.0(0.8)	0.07(0.02)	0.006(0.001)
844(20)	8(21)	0.009(0.068)	844(20)	8.7(0.6)	0.010(0.002)	844(20)	8(1)	0.010(0.007)
19.4(0.9)	688(1)	35(7)	19.4(0.9)	437(11)	22(43)	19.4(0.9)	456(9)	24(10)
12(2)	1934(2)	47(14)	12(2)	1196(31)	29(122)	12(2)	2121(20)	52(27)
4.6(0.2)	260.5(0.2)	56(6)	4.6(0.2)	154(7)	34(63)	4.6(0.2)	155(3)	34(9)
18.5(0.9)	1181(1)	64(13)	18.5(0.9)	674(25)	36(190)	18.5(0.9)	659(15)	36(21)
3.5(0.2)	280.5(0.2)	80(7)	3.5(0.2)	149(5)	42(136)	3.5(0.2)	143(5)	41(18)
4.2(0.2)	64.5(0.2)	15(2)	4.2(0.2)	35(2)	8(7)	4.2(0.2)	32.4(0.7)	8(1)
2.5(0.8)	199(1)	80(39)	2.5(0.8)	111(21)	45(468)	2.5(0.8)	101(13)	40(56)
1.9(0.2)	171.5(0.3)	90(17)	1.9(0.2)	88(5)	46(123)	1.9(0.2)	85(4)	45(20)
0.5(0.2)	85.0(0.2)	167(47)	0.5(0.2)	45(4)	88(317)	0.5(0.2)	44(2)	87(35)
0.36(0.2)	64.0(0.2)	178(60)	0.36(0.2)	34(3.1)	95(209)	0.36(0.2)	30(1)	86(34)
0.05(0.07)	8.45(0.07)	168(53)	0.05(0.07)	4.5(0.4)	91(119)	0.05(0.07)	4.0(0.2)	80(27)
8.1(0.6)	—	—	8.1(0.6)	—	—	8.1(0.6)	—	—

M4 site. The large ion lithophile (LIL) elements such as K, Rb, and Sr are all found in the much larger A site. It would appear that Li, due to its small ionic radius, partitions into the M1, M2 or M3 site. For plagioclase, the HFSE are partitioned into the tetrahedral (T) site, whereas all other elements reside in the much larger M site. In orthopyroxene, the smaller M1 site contains the HFSE and (apparently) Li, whereas the larger M2 site contains the REE and LIL elements. Finally, the large Ca1 site in apatite contains the LIL elements and Li, whereas the smaller Ca2 site contains the REEs and HFSEs.

Sisson (1994) reported empirical relationships for determining hornblende-liquid REE D values based solely on the Ca content of the hornblende. Figure 7 compares our observed hornblende REE D values with those predicted by the empirical relations. The results indicate that our D values compare favorably with the predicted values for the LREEs and MREEs but unfavorably for the HREEs where the observed values are much greater than the predicted values. This discrepancy is significant for the predicted patterns display an enrichment of MREEs relative to HREE D values that are considered characteristic of

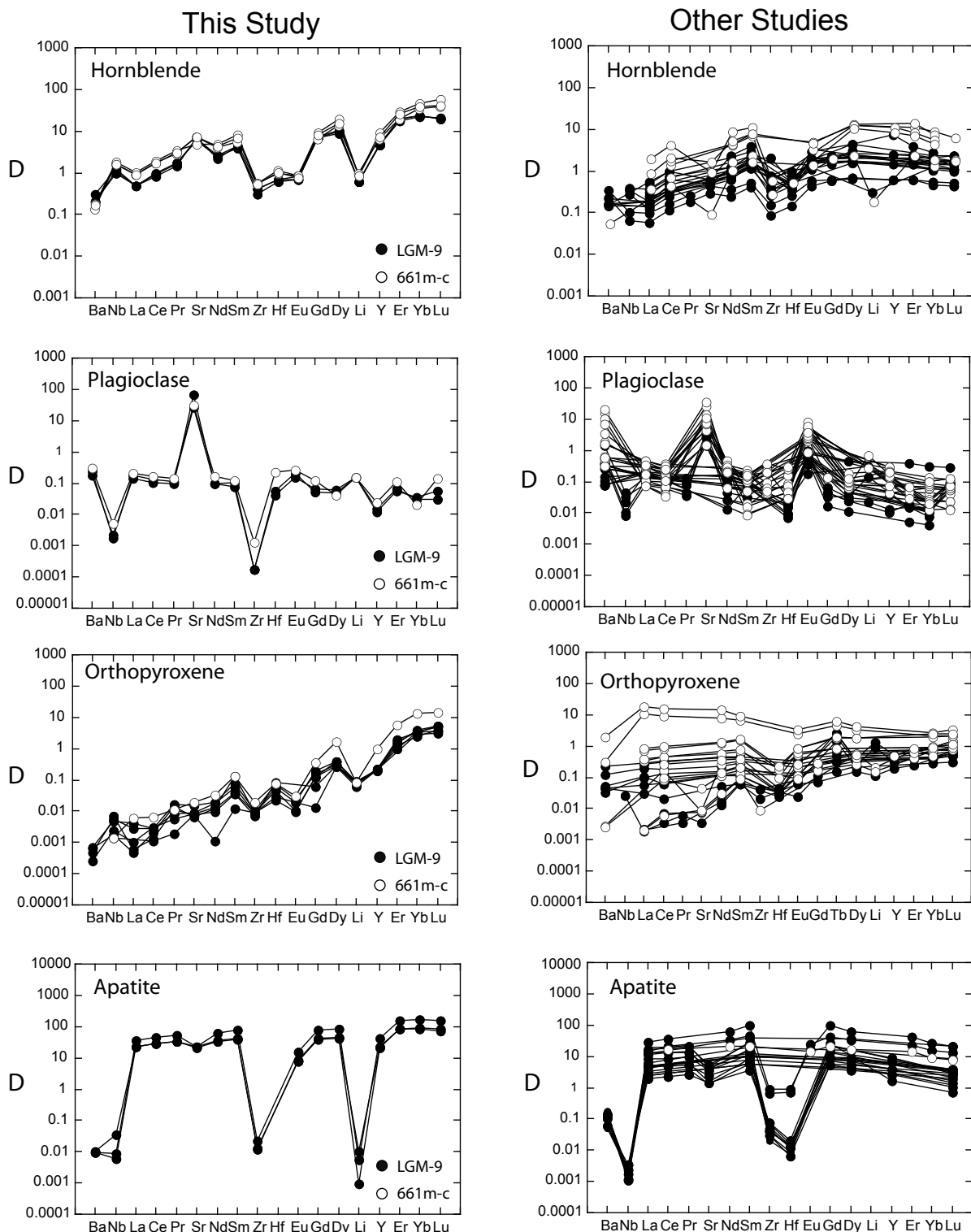


FIGURE 4. Multi-element diagrams showing all measured D values from this study. Shown for comparison are published D values from other studies for which the SiO₂ content of the liquid (i.e., natural matrix or glass, experimental liquid) was reported. In the latter, systems for which the liquid SiO₂ content was >70 wt% are shown as open circles. Data sources include Bacon and Druitt (1988), Dalpe and Baker (2000), Dostal et al. (1983), Klein et al. (1997), Luhr and Carmichael (1980), Luhr et al. (1984), Nagasawa and Schnetzler (1971), Sisson (1991, 1994), Dunn and Senn (1994), Nash and Crecraft (1985), Streck and Grunder (1997), Mahood and Hildreth (1983), Fujimaki (1986), Watson and Green (1982), and Prowatke and Klemme (2006).

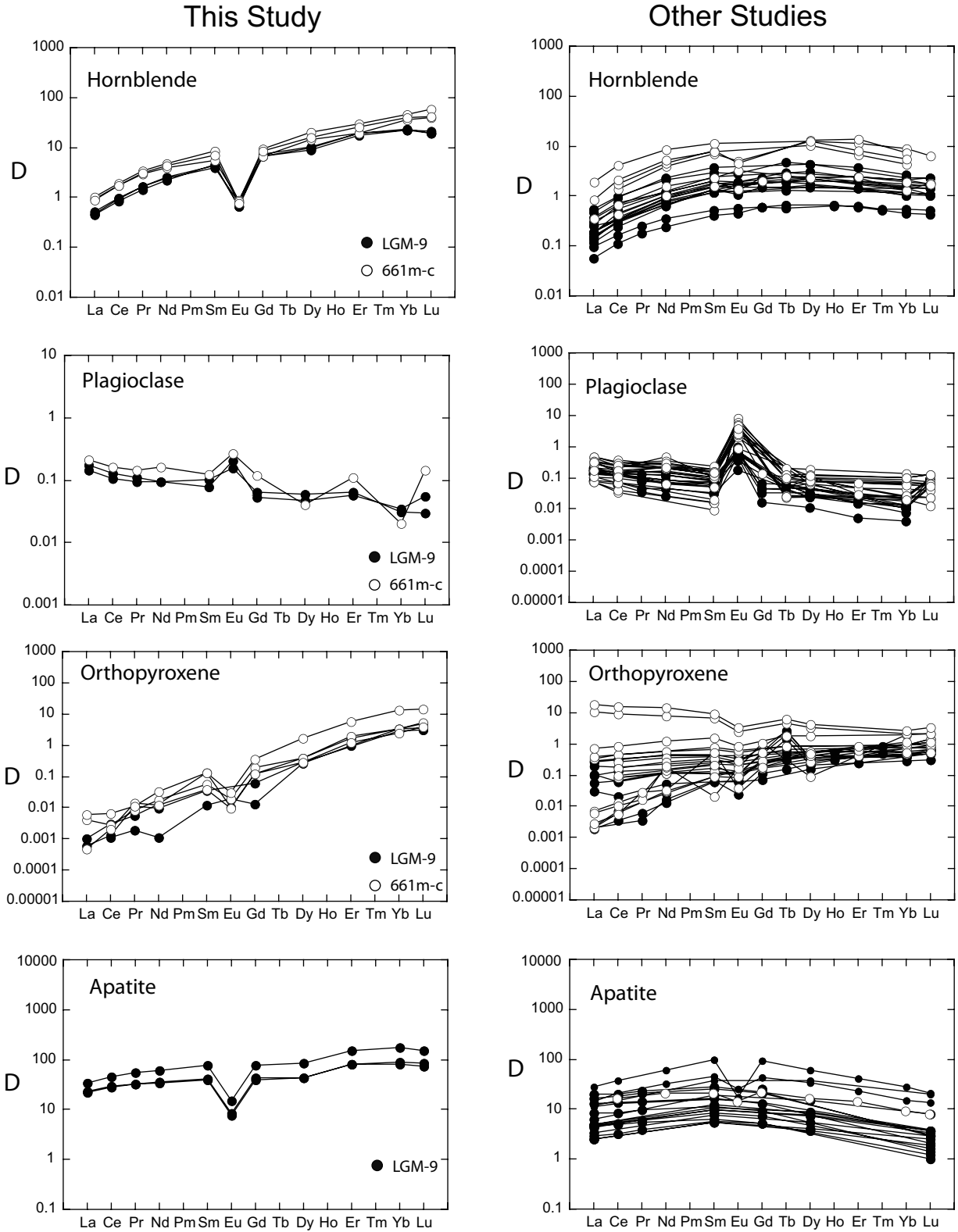


FIGURE 5. REE diagrams showing all measured D values from this study along with those from other studies. In the latter, systems for which the liquid SiO₂ content was >70 wt% are shown as open circles. Data sources are the same as those listed for Figure 4.

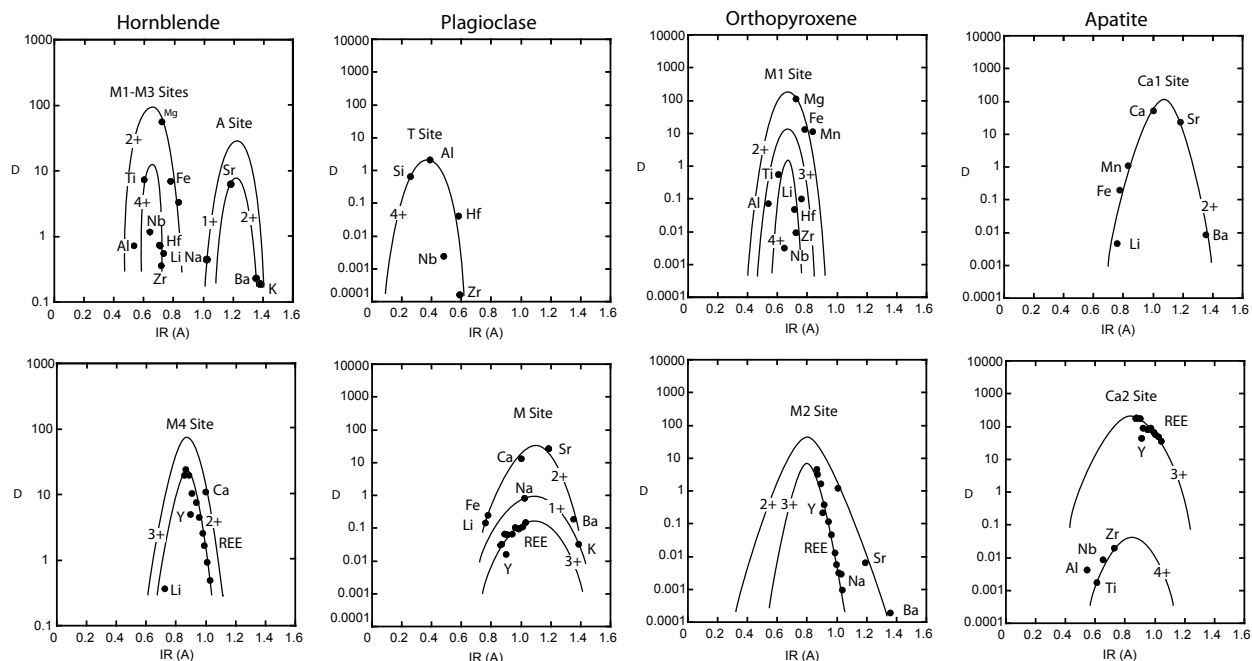


FIGURE 6. Trace element D vs. ionic-radius diagrams (i.e., Onuma Diagrams) for a single hornblende (LGM-9 Hbd C), plagioclase, (LGM-9 Plag-B) orthopyroxene (LGM-OpX A) and apatite (LGM-9 apatite 1) crystal from inclusion LGM-9. Where appropriate, major element D values have been calculated from the major element glass and mineral rim data. For a given mineral and cation site, the solid curves represent qualitative parabolic “fits” to elements of the same charge.

hornblende. Our data, on the other hand, display a steady increase in REE D values that is reminiscent of those determined for hornblende crystals in granodiorites and granites of the Sierra Nevada batholith (Dodge et al. 1982; Sawka 1988; Sawka et al. 1990). Sisson (1994) suggested that the granodiorite and granite REE D data were due to partial re-equilibration with residual liquids depleted in the MREEs due to crystallization of titanite. Our liquid data (Fig. 2) show no such depletion in the MREEs indicating that this is not a plausible explanation for our data. Sisson’s (1994) calibration was based on hornblende-liquid pairs that ranged from 53 to 72 wt% SiO₂ in the liquid. Our data are derived from liquids ranging from ~73 to 74% SiO₂ suggesting that the predictive relations of Sisson (1994) should be restricted to the liquid SiO₂ range over which they were calibrated.

It has long been recognized but under-appreciated that, for many minerals, D values for any given trace element systematically increase with liquid SiO₂ content. This behavior is emphasized in Figure 8, which shows reported REE D values vs. liquid SiO₂ content for representative light (La), middle (Sm), and heavy (Lu) REEs. Both hornblende and apatite display significant increases in D value, whereas plagioclase and orthopyroxene do not. This differing behavior can be explained as follows. Increasing D value with increasing liquid SiO₂ is normally attributed to a decrease in the ratio of non-bridging oxygen (NBO) to tetrahedral cation site (T) (NBO/T) in the liquid that, in turn, reduces the number of free O atoms with which a trace element can coordinate. In short, the solubility of the trace element in the melt decreases so the only place for the element to go is into the coexisting minerals. An important aspect of Figure 8 is that the effect of increasing liquid SiO₂ on REE D value is

most pronounced for hornblende and apatite and much less so for plagioclase and orthopyroxene. These differences undoubtedly reflect fundamental thermodynamic controls involving the solution properties of both mineral and liquid. However, such considerations are beyond the scope of the present study. Also noteworthy is the significant disagreement between the SIMS-based data for La and Sm orthopyroxene D values (including those of this study) for high-SiO₂ liquids and those generated by bulk analysis of natural phenocryst matrix pairs. Given the close correspondence among the SIMS data generated by ours and another unrelated study, we conclude that the SIMS data are of

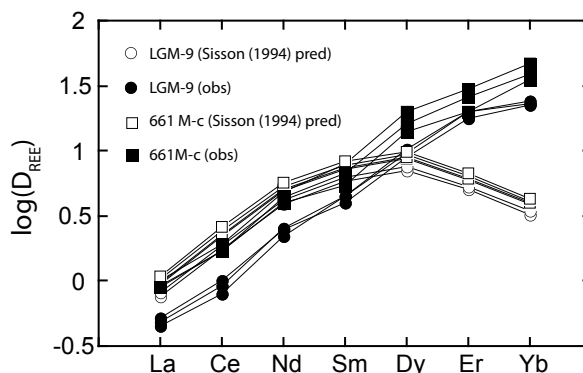


FIGURE 7. A comparison of amphibole D values for selected REEs calculated by the method of Sisson (1994) with the observed values from this study. There is good agreement for the LREEs to MREEs but poor agreement for the HREEs.

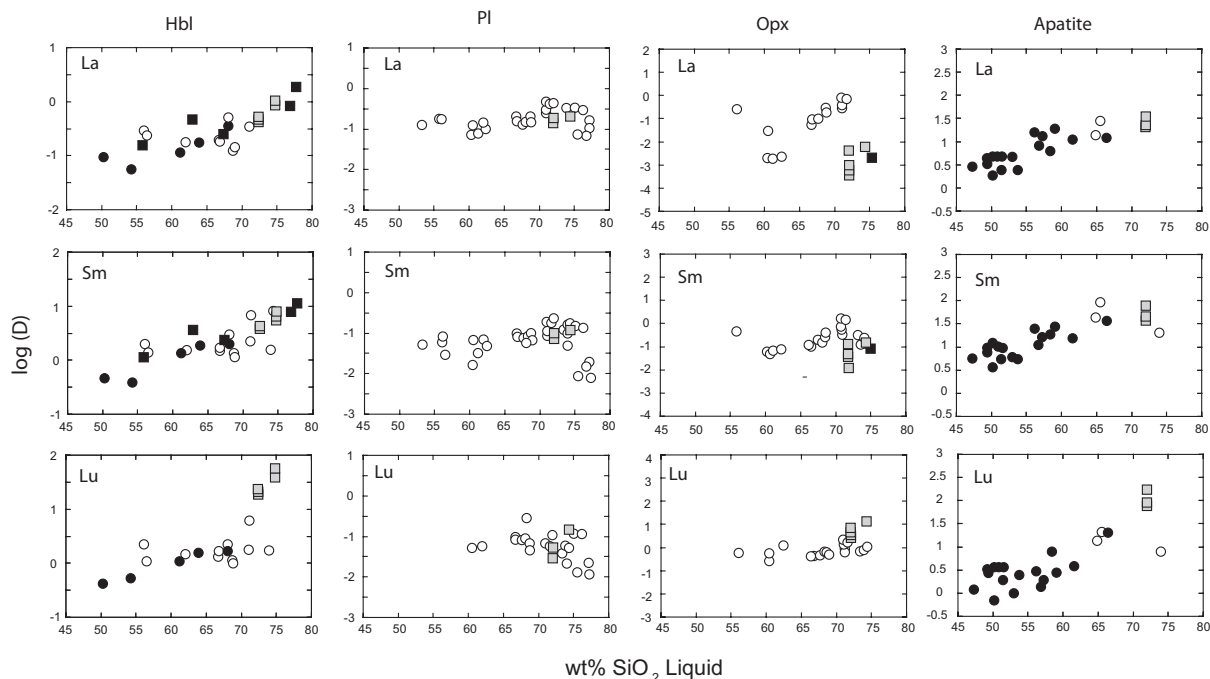


FIGURE 8. Log D vs. liquid SiO₂ diagrams showing data from this and previously published studies. Data are shown for selected light, middle, and heavy REEs. The symbols represent different types of partition coefficients and include natural phenocryst matrix (open circle), experimental (closed circle), and SIMS (closed square). Data from the present study are shown as light gray squares. Data sources include (Bacon and Druitt 1988; Dalpe and Baker 2000; Dostal et al. 1983; Fujimaki 1986; Klein et al. 1997; Luhr and Carmichael 1980; Luhr et al. 1984; Nagasawa and Schnetzler 1971; Sisson 1991, 1994).

better quality and that the significantly higher phenocryst-matrix D values are incorrect and should be used with caution. Finally, it is strongly urged that any future studies of crystallization or melting that involve modeling of the REEs, take into account the significant melt composition control on D values for many important mineral phases.

ACKNOWLEDGMENTS

The first author thanks the Pheasant Memorial Laboratory of the Institute for Study of the Earth's Interior for making all of their analytical facilities available for this study. Tom Sisson and John Longhi are thanked for their critical but invaluable reviews. This work was funded in part by NSF grant EAR-0946284 (J.G.B.).

REFERENCES CITED

- Bacon, C.R. and Druitt, T.H. (1988) Compositional evolution of the zoned calc-alkaline magma chamber of Mount Mazama, Crater Lake, Oregon. *Contributions to Mineralogy and Petrology*, 98, 224–256.
- Brophy, J.G., Dorais, M.J., Donnelly-Nolan, J.M., and Singer, B.S. (1996) Plagioclase zonation styles in hornblende gabbro inclusions from Little Glass Mountain, Medicine Lake volcano, California: implications for fractionation mechanisms and the formation of composition gaps. *Contributions to Mineralogy and Petrology*, 126, 121–136.
- Dalpe, C. and Baker, D.R. (2000) Experimental investigation of large ion lithophile element, high field strength element, and rare earth element partitioning between calcic amphibole and basaltic melts; the effects of pressure and oxygen fugacity. *Contributions to Mineralogy and Petrology*, 140, 233–250.
- Deering, C.D., Cole, J.W., and Vogel, T.A. (2008) A rhyolite compositional continuum governed by lower crustal source conditions in the Taupo Volcanic Zone, New Zealand. *Journal of Petrology*, 49, 2245–2276.
- Dodge, F.C.W., Millard, H.T. and Elsheimer, H.N. (1982) Compositional variations and abundances of selected elements in granitoid rocks and constituent minerals, central Sierra Nevada batholiths, California. U.S. Geological Survey Professional Paper, 1248, 24 pp.
- Donnelly-Nolan, J.M., Champion, D.E., Miller, C.D., Grove, T.L. and Trimble, D.A. (1990) Post-11,000 year volcanism at Medicine Lake Volcano, Cascade Range, Northern California. *Journal of Geophysical Research*, 95, 19693–19704.
- Dostal, J., Dupuy, J., Carron, J.P., Le Guen de Kerniezon, M., and Maury, R.C. (1983) Partition coefficients of trace elements: application to volcanic rocks of St. Vincent, West Indies. *Geochimica et Cosmochimica Acta*, 47, 525–533.
- Dunn, T. and Senn, C. (1994) Mineral/matrix coefficients for orthopyroxene, plagioclase and olivine in basaltic to andesitic systems: a combined analytical and experimental study. *Geochimica et Cosmochimica Acta*, 47, 717–753.
- Ewart, A. and Griffin, W.L. (1994) Application of proton-microprobe data to trace element partitioning in volcanic rocks. *Chemical Geology*, 117, 251–284.
- Fujimaki, H. (1986) Partition coefficients of Hf, Zr and REE between zircon, apatite and liquid. *Contributions to Mineralogy and Petrology*, 94, 42–45.
- Grove, T.L. and Donnelly-Nolan, J.M. (1986) The evolution of young silicic lavas at Medicine Lake Volcano, California: Implications for the origin of compositional gaps in calc-alkaline series lavas. *Contributions to Mineralogy and Petrology*, 92, 281–302.
- Grove, T.L., Donnelly-Nolan, J.M., and Housh, T.B. (1997) Magmatic processes that generated the rhyolite of Glass Mountain, Medicine Lake Volcano, N. California. *Contributions to Mineralogy and Petrology*, 127, 205–223.
- Klein, M., Stosch, H.G., and Seck, H.A. (1997) Partitioning of high field strength and rare earth elements between amphibole and quartz-dioritic to tonalitic melts: an experimental system. *Chemical Geology*, 138, 257–271.
- Lange, R.A., Frey, H.M., and Hector, J. (2009) A thermodynamic model for the plagioclase-liquid hygrometer/thermometer. *American Mineralogist*, 94, 494–506.
- Leake, B.E., Woolley, A.R., Arps, C.E.S., Birch, W.D., Gilbert, M.C., Hawthorne, F.C., Kato, A., Kisch, H.J., Krivovichev, V.G., Linthout, K., and others. (1997) Nomenclature of amphiboles: report of the subcommittee on amphiboles of the International Mineralogical Association, Commission on New Minerals and Mineral Names. *Canadian Mineralogist*, 35, 219–246.
- Luhr, J.F. and Carmichael, I.S.E. (1980) The Colima Volcanic Complex, Mexico. *Contributions to Mineralogy and Petrology*, 71, 343–372.
- Luhr, J.F., Carmichael, I.S.E., and Varekamp, J.C. (1984) The 1982 eruptions of El Chichon Volcano, Chiapas, Mexico: mineralogy and petrology of the anhydrite bearing pumices. *Journal of Volcanology and Geothermal Research*, 23, 69–108.
- Mahood, G. and Hildreth, W. (1983) Large partition coefficients for trace elements in high-silica rhyolites. *Geochimica et Cosmochimica Acta*, 47, 11–30.

- Makishima, A. and Nakamura, E. (1997) Suppression of matrix effect in ICP-MS by high power operation of ICP: Application to precise determination of Rb, Sr, Y, Cs, Ba, REE, Pb, Th and U at ng/g levels in a few milligram silicate sample. *Geostandards Newsletter*, 21, 307–319.
- Makishima, A., Nakamura, E., and Nakano, T. (1999) Determination of zirconium, niobium, hafnium and tantalum at ng g⁻¹ levels in geological materials by direct nebulization of sample HF solution into FI-ICP-MS. *Geostandards Newsletter*, 23, 7–20.
- Mertzmann, S.A. and Williams, R.G. (1981) Genesis of recent silicic magmatism in the Medicine Lake Highland, California: Evidence for cognate inclusions found at Little Glass Mountain. *Geochimica et Cosmochimica Acta*, 45, 1463–1478.
- Moriguti, T., Makishima, A., and Nakamura, E. (2004) Determination of lithium contents in silicates by isotope dilution ICP-MS and its evaluation by isotope dilution thermal ionisation mass spectrometry. *Geostandards and Geoanalytical Research*, 28, 371–382.
- Nagasawa, H. and Schnetzler, C.C. (1971) Partitioning of rare earth, alkali and alkaline earth elements between phenocrysts and acidic igneous magma. *Geochimica et Cosmochimica Acta*, 35, 953–968.
- Nakamura, E. and Kushiro, I. (1998) Trace element diffusion in jadeite and diopside melts at high pressure and its geochemical implication. *Geochimica et Cosmochimica Acta*, 62, 3151–3160.
- Nash, W.P. and Crecraft, H.R. (1985) Partition coefficients for trace elements in felsic magmas. *Geochimica et Cosmochimica Acta*, 49, 2309–2322.
- Onuma, H., Higuchi, H., Wakita, H., and Nagasawa, H. (1968) Trace element partition between two pyroxenes and the host lava. *Earth and Planetary Science Letters*, 5, 47–51.
- Prowatke, S. and Klemme, S. (2006) Trace element partitioning between apatite and silicate melts. *Geochimica et Cosmochimica Acta*, 70, 4513–4527.
- Ridolfi, F., Renzulli, A., and Matteo, P. (2010) Stability and chemical equilibrium of amphibole in calc-alkaline magmas: an overview, new ghermobarometric formulations and application to subduction-related volcanoes. *Contributions to Mineralogy and Petrology*, 160, 45–66.
- Sawka, W.N. (1988) REE and trace element variations in accessory minerals and hornblende from the strongly zoned McMurry Meadows pluton, California. *Transactions Royal Society of Edinburgh*, 79, 157–168.
- Sawka, W.N., Chappel, B.W., and Kistler, R.W. (1990) Granitoid compositional zoning by side-wall boundary layer differentiation: Evidence from the Palisade Crest intrusive suit, central Sierra Nevada, California. *Journal of Petrology*, 31, 519–553.
- Sisson, T.W. (1991) Pyroxene-high silicic rhyolite trace element partition coefficients measured by ion microprobe. *Geochimica et Cosmochimica Acta*, 56, 2133–2136.
- (1994) Hornblende-melt trace element partitioning measured by ion microprobe. *Chemical Geology*, 117, 331–344.
- Spencer, K.J. and Lindsley, D.H. (1981) A solution model for co-existing iron-titanium oxides. *American Mineralogist*, 66, 1189–1201.
- Streck, M.J. and Grunder, A.L. (1997) Compositional gradients and gaps in high-silica rhyolites of the Rattlesnake Tuff, Oregon. *Journal of Petrology*, 38, 133–163.
- Watson, E.B. and Baxter, E.R. (2007) Diffusion in solid-earth systems. *Earth and Planetary Science Letters*, 253, 307–327.
- Watson, E.B. and Green, T.H. (1982) Apatite/liquid partition coefficients for the rare earth elements and strontium. *Earth and Planetary Science Letters*, 56, 405–421.
- Yokoyama, T., Makishima, A., and Nakamura, E. (1999) Evaluation of the coprecipitation of incompatible trace elements with fluoride during silicate rock dissolution by acid digestion. *Chemical Geology*, 157, 175–187.

MANUSCRIPT RECEIVED APRIL 11, 2011

MANUSCRIPT ACCEPTED JULY 26, 2011

MANUSCRIPT HANDLED BY GEORGE MORGAN